Supplementary Materials

Monodisperse $NaYbF_4:Tm^{3+}/NaGdF_4$ core/shell nanocrystals with near-infrared to near-infrared upconversion photoluminescence and magnetic resonance properties

Guanying Chen,[†‡] Tymish Y. Ohulchanskyy,[†]* Wing Cheung Law,[†] Hans Ågren,[‡] and Paras N. Prasad[†]*

[†]Institute for Lasers, Photonics, and Biophotonics, The State University of New York University at Buffalo, Buffalo, New York 14260

[‡]Department of Theoretical Chemistry, Royal Institute of Technology, S-10691 Stockholm, Sweden
*Corresponding Authors. E-mails: tyo2@buffalo.edu, pnprasad@buffalo.edu

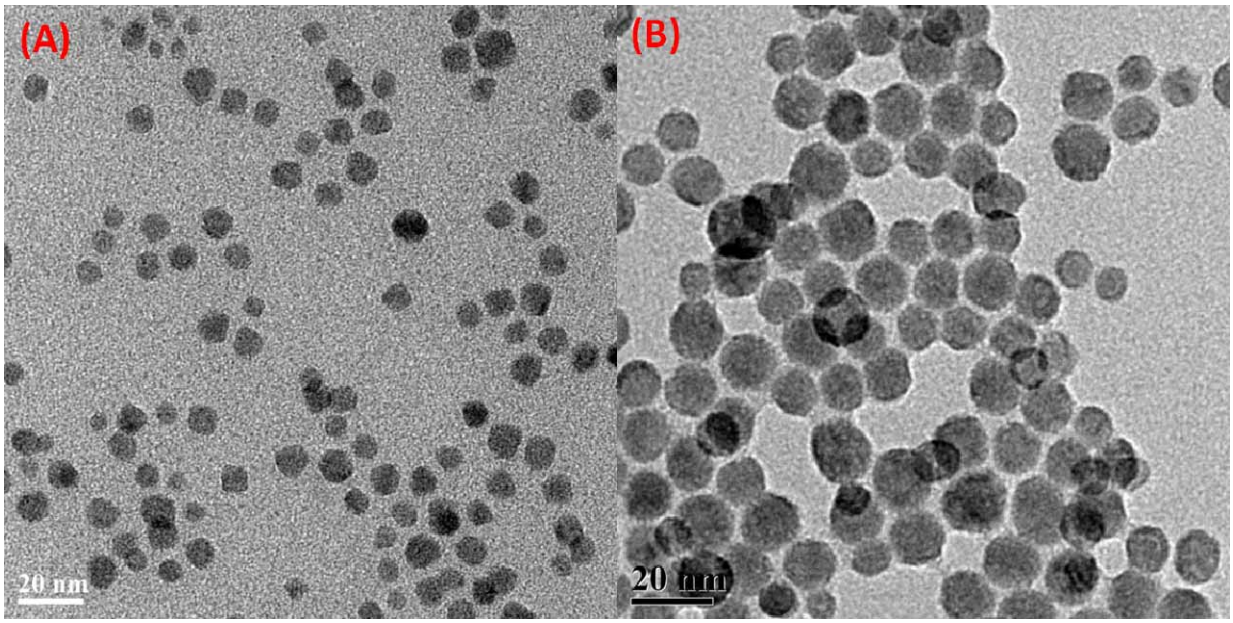

Figure S1. Transmission electron images with higher magnification times for (A) $NaYbF_4$:2% Tm^{3+} core and (B) ($NaYbF_4$:Tm 2%)/$NaGdF_4$ core/shell powders.

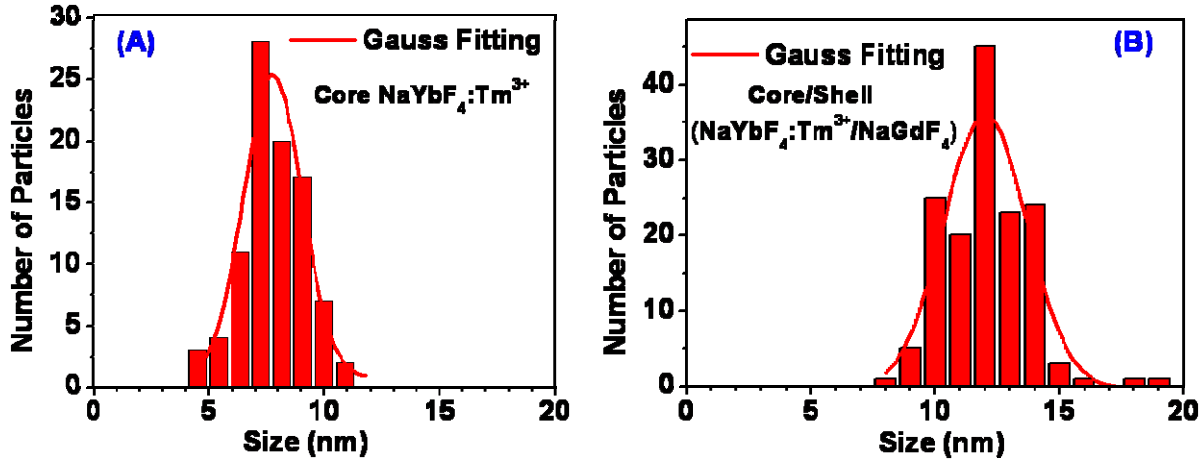

Figure S2. Histograms of the size distribution of (A) $NaYbF_4$:2% Tm^{3+} core and (B) ($NaYbF_4$:Tm 2%)/$NaGdF_4$ core/shell nanocrystals.

Table S1. *d*-spacing values for $NaYbF_4$:2% Tm^{3+} nanocrystals determined via selected area electron diffraction (SAED) and standard x-ray diffraction (XRD) pattern of cubic $NaYbF_4$ of JCPDS 77-2043. As shown in Table S1, all the *d*-spacing values of $NaYbF_4$:2% Tm^{3+} nanocrystals agree well with the standard x-ray diffraction (XRD) pattern of cubic $NaYbF_4$ of JCPDS 77-2043

	d-spacing values (nm)	
h k l	$NaYbF_4$:Tm^{3+} 2% (SAED)	Standard XRD pattern JCPDS 77-2043
(111)	0.319	0.313
(200)	0.273	0.271
(220)	0.194	0.192
(311)	0.166	0.163
(222)	0.159	0.156

Table S2. *d*-spacing values for $NaYbF_4:Tm^{3+}/NaGdF_4$ core/shell nanocrystals derived from the SAED pattern and the standard XRD pattern of hexagonal $NaGdF_4$ of JCPDS 77-2043. As shown in Table S2, nearly all the *d*-spacing values of $NaYbF_4:Tm^{3+}/NaGdF_4$ core/shell nanocrystals agree well with the standard x-ray diffraction (XRD) pattern of hexagonal $NaGdF_4$ of JCPDS 77-2043. It should be noted that the *d*-spacing value of the (100) crystal plane deviate a lot from that of the standard hexagonal $NaGdF_4$ of JCPDS 77-2043. This might be because the crystal of the $NaGdF_4$ shell adapt itself to grow (100) plane on top of the $NaYbF_4$ core along the (200) direction.

	d-spacing values (nm)	
h k l	$NaYbF_4:Tm^{3+}$ 2% (SAED)	standard XRD pattern JCPDS 27-0699
(100)	0.540	0.521
(110)	0.308	0.301
(200)	0.267	0.260
(111)	0.238	0.231
(201)	0.216	0.212
(210)	0.202	0.197
(211)	0.180	0.173

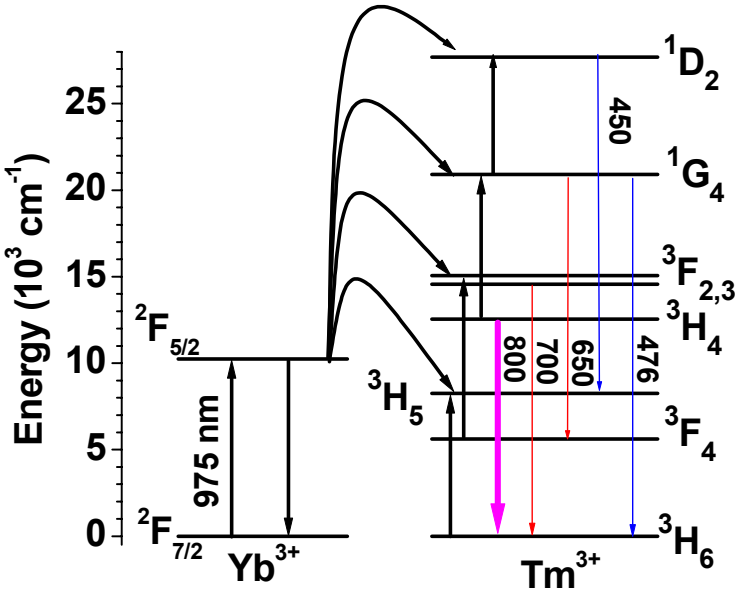

Figure S3. Energy level diagrams of Yb^{3+} and Tm^{3+} ions as well as the proposed upconversion mechanisms. Figure S3 shows the energy levels of the involved Yb^{3+} and Tm^{3+} ions as well as the proposed UC pathways under diode laser excitation of 975 nm. The pump laser photons of 975 nm can only excite the Yb^{3+} ion, because the Tm^{3+} ion has no such excited level above its ground state. As pictured in Figure S3, the first energy transfer process from the Yb^{3+} to the Tm^{3+} ion excites the $^3H_6$ to the $^3H_5$ state with the redundant energy dissipated by phonons. Subsequently, the Tm^{3+} ion relaxes nonradiatively to the lower $^3F_4$ state and further populates the $^3F_{2,3}$ state through a second energy transfer process from the Yb^{3+} to the Tm^{3+} ion. The weak UC emission at 700 nm is then generated by radiative decay from the $^3F_{2,3}$ state to the ground state. Additionally, the strong NIR emission at 802 nm arises from the $^3H_4 \rightarrow {}^3H_6$ transition where the $^3H_4$ state is populated by the efficient nonradiative relaxation from the $^3F_{2,3}$ state. The third process from the Yb^{3+} to the Tm^{3+} ion excites the $^3H_4$ to the $^1G_4$ state from which the 476 and 650 nm UC emissions were generated corresponding to the $^1G_4 \rightarrow {}^3H_6$ and $^1G_4 \rightarrow {}^3F_4$ transitions,

respectively. Then, the ions at the $^1G_4$ state can be further promoted to the $^1D_2$ state by the fourth process from the Yb^{3+} to the Tm^{3+} ion, which emits UC emission at 450 nm of the $^1D_2 \rightarrow {}^3F_4$ transition.